

Isomerism of $[\text{Ru}(\eta^3\text{-allyl})\text{Cl}(\text{CO})(\text{PPh}_3)_2]$

Peng Xue, Siwei Bi, Herman H. Y. Sung, Ian D. Williams, Zhenyang Lin,* and Guochen Jia*

Department of Chemistry and Open Laboratory of Chirotechnology of the Institute of Molecular Technology for Drug Discovery and Synthesis, The Hong Kong University of Science and Technology, Clear Water Bay, Kowloon, Hong Kong

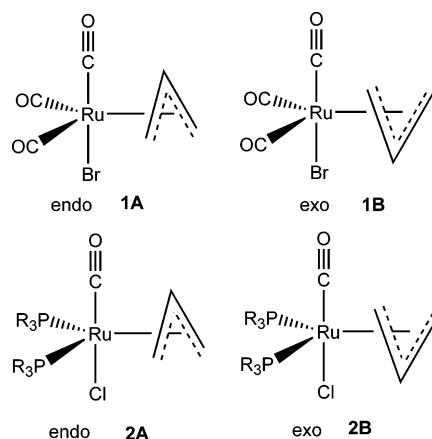
Received May 17, 2004

Treatment of $[\text{RuHCl}(\text{CO})(\text{PPh}_3)_3]$ with $\text{CH}_2=\text{C}=\text{CMe}_2$ produced the new allyl complex $[\text{Ru}(\eta^3\text{-CH}_2\text{CHCMe}_2)\text{Cl}(\text{CO})(\text{PPh}_3)_2]$, which slowly isomerizes to $[\text{Ru}(\eta^3\text{-CH}_2\text{CMeCHMe})\text{Cl}(\text{CO})(\text{PPh}_3)_2]$ in both solution and the solid state. While both endo and exo isomers can be observed by solution NMR for the allyl complex $[\text{Ru}(\eta^3\text{-CH}_2\text{CHCMe}_2)\text{Cl}(\text{CO})(\text{PPh}_3)_2]$, only the endo isomer was detected for other related analogous allyl complexes $[\text{Ru}(\eta^3\text{-allyl})\text{Cl}(\text{CO})(\text{PPh}_3)_2]$ (e.g. allyl = $\text{CH}_2\text{CMeCHMe}$, CH_2CHCHPh). The isomeric behavior has been investigated by computational chemistry. The theoretical calculations show that the metal– η^3 -allyl interaction in an endo isomer of $[\text{Ru}(\eta^3\text{-allyl})\text{Cl}(\text{CO})(\text{PR}_3)_2]$ complexes is stronger than that in an exo isomer, because the structural arrangement provides an optimal situation to maximize the $\text{Ru}(\text{d})$ -to- $\text{CO}(\pi^*)$ back-bonding interaction. However, substituents at the η^3 -allyl ligand also play an important role in determining the relative stability. It was found that an anti substituent (with respect to the central allylic substituent) at one of the terminal carbons destabilizes the endo isomer more significantly and therefore makes the endo and exo isomers comparable in terms of their relative stabilities. A syn substituent at one of the terminal carbons is, however, found to have a negligible effect on the relative stability. The endo–exo interconversion was found to proceed by intervention of η^1 -allyl intermediates instead of a direct η^3 -allyl rotation.

Introduction

Ruthenium η^3 -allyl complexes have attracted much attention, because they can mediate organometallic and catalytic reactions.¹ It is well established that π -allyl complexes can exist in two isomers due to the relative orientations of the allyl ligands.^{1d,2} Understanding the factors controlling the relative energy of the isomers should help to understand the regio- and stereochemistry of reactions mediated by π -allyl complexes.

This work concerns the isomerism of ruthenium η^3 -allyl complexes of the type $[\text{Ru}(\eta^3\text{-allyl})\text{Cl}(\text{CO})(\text{L})_2]$. It has been demonstrated that $[\text{Ru}(\eta^3\text{-allyl})\text{Br}(\text{CO})_3]$ exists as both endo (**1A**) and exo (**1B**) isomers in a ratio of 40:1 in CDCl_3 .³ In the endo isomer, the central allylic hydrogen points toward the CO; in the exo isomer, the central allylic hydrogen points toward the halide. An



early theoretical study showed that the endo isomer is ca. 1.7 kcal/mol more stable than the exo isomer.⁴ A number of ruthenium η^3 -allyl complexes $[\text{Ru}(\eta^3\text{-allyl})\text{Cl}(\text{CO})(\text{PR}_3)_2]$ ($(\text{PR}_3)_2 = (\text{PPh}_3)_2$,⁵ $(\text{PMe}_2\text{Ph})_2$,⁶ dppf)⁷ have also been prepared. In principle, these complexes

* To whom correspondence should be addressed. E-mail: chzlin@ust.hk (Z.L.); chjiag@ust.hk (G.J.).

(1) See for example: (a) Yamamoto, Y.; Nakagai, Y.; Itoh, K. *Chem. Eur. J.* **2004**, *10*, 231. (b) Mbaye, M. D.; Demerseman, B.; Renaud, J. L.; Toupet, L.; Bruneau, C. *Angew. Chem., Int. Ed.* **2003**, 5066. (c) Sasabe, H.; Nakanishi, S.; Takata, T. *Inorg. Chem. Commun.* **2003**, *6*, 1140. (d) Braun, T.; Münch, G.; Windmüller, B.; Gevert, O.; Laubender, M.; Werner, H. *Chem. Eur. J.* **2003**, 2516. (e) Chamberlain, B.; Duckett, S. B.; Lowe, J. P.; Mawby, R. J.; Stott, J. C. *Dalton* **2003**, 2603. (f) Castro, A.; Turner, M. L.; Maitlis, P. M. *J. Organomet. Chem.* **2003**, 674, 45. (g) Kondo, T.; Ono, H.; Satake, N.; Mitsudo, T.; Watanabe, Y. *Organometallics* **1995**, *14*, 1945.

(2) See for example: (a) Norman, D. W.; Ferguson, M. J.; Stryker, J. M. *Organometallics* **2004**, *23*, 2015. (b) Cedeno, D. L.; Weitz, E. *Organometallics* **2003**, *22*, 2652. (c) Takao, Y.; Takeda, T.; Watanabe, J.; Setsune, J. *Organometallics* **2003**, *22*, 233. (d) Staveren, D. R.; Bill, E.; Bothe, E.; Bühl, M.; Weyhermüller, T.; Metzler-Nolte, N. *Chem. Eur. J.* **2002**, *8*, 1649.

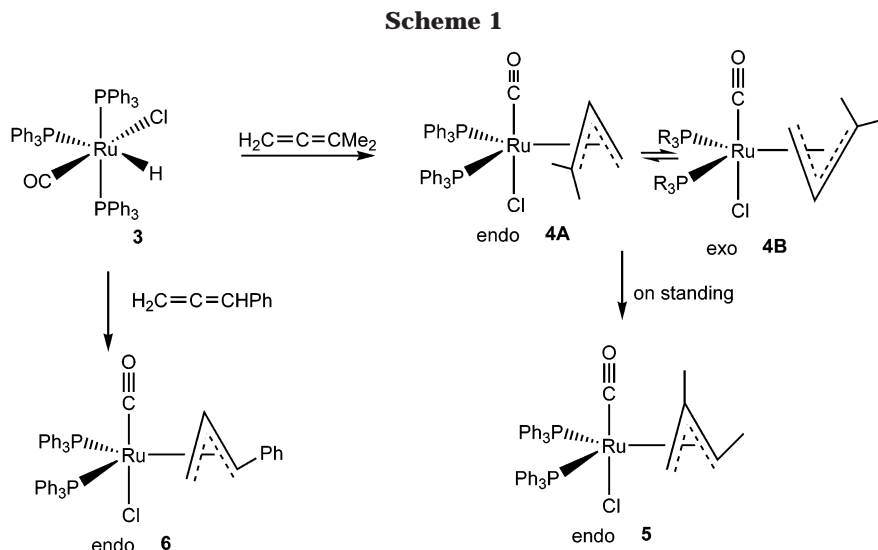
(3) Wu, Y. M.; Wrighton, M. S. *Organometallics* **1988**, *7*, 1839.

(4) Sakaki, S.; Ohki, T.; Takayama, T.; Sugimoto, M.; Kondo, T.; Mitsudo, T. *Organometallics* **2001**, *20*, 3145.

(5) (a) Sasabe, H.; Nakanishi, S.; Takata, T. *Inorg. Chem. Commun.* **2002**, *5*, 177. (b) Hiraki, K.; Matsunaga, T.; Kawano, H. *Organometallics* **1994**, *13*, 1878. (c) Hill, A. F.; Ho, C. T.; Wilton-Ely, D. E. T. *Chem. Commun.* **1997**, 2207. (d) Hiraki, K.; Ochi, N.; Sasada, Y.; Hayashida, H.; Fuchita, Y.; Yamanaka, S. *J. Chem. Soc., Dalton Trans.* **1985**, 873.

(6) Barnard, C. F. J.; Daniels, B. J. A.; Holland, P. R.; Mawby, R. J. *J. Chem. Soc., Dalton Trans.* **1980**, 2418.

(7) Cadierno, V.; Crochet, P.; Diez, J.; Garcia-Garrido, S. E.; Gimeno, J. *Organometallics* **2003**, *22*, 5226.



could also have the two isomers **2A** and **2B**. However, the expected isomerism was not observed previously and only the endo isomer was detected in solution for the reported ruthenium η^3 -allyl complexes of the type $[\text{Ru}(\eta^3\text{-allyl})\text{Cl}(\text{CO})(\text{PR}_3)_2]$.

During the course of investigating the reactivities of $[\text{RuHCl}(\text{CO})(\text{PPh}_3)_3]$ toward allenes, we have prepared the allyl complex $[\text{Ru}(\eta^3\text{-CH}_2\text{CHCMe}_2)\text{Cl}(\text{CO})(\text{PPh}_3)_2]$ and found that the allyl complex $[\text{Ru}(\eta^3\text{-CH}_2\text{CHCMe}_2)\text{Cl}(\text{CO})(\text{PPh}_3)_2]$ does exist in two isomers in solution. The main purpose of this work is to address the question why two isomers were observed for $[\text{Ru}(\eta^3\text{-CH}_2\text{CHCMe}_2)\text{Cl}(\text{CO})(\text{PPh}_3)_2]$ but only one isomer was observed for other related reported allyl complexes $[\text{Ru}(\eta^3\text{-allyl})\text{Cl}(\text{CO})(\text{PR}_3)_2]$.

Results and Discussion

Synthesis of Allyl Complexes. Treatment of $[\text{RuHCl}(\text{CO})(\text{PPh}_3)_3]$ (**3**) with $\text{CH}_2=\text{C}=\text{CMe}_2$ produced the new allyl complex $[\text{Ru}(\eta^3\text{-CH}_2\text{CHCMe}_2)\text{Cl}(\text{CO})(\text{PPh}_3)_2]$ (**4**) (Scheme 1). Related complexes of the same metal fragment with other allyl ligands (e.g. CH_2CHCH_2 , $\text{CH}_2\text{-CMeCH}_2$, MeCHCHCHMe , $\text{EtCHCHCHCO}_2\text{Et}$) are known.⁵ In all the reported complexes, the substituents at the terminal allylic carbons are syn to the central allylic proton or substituent. Complex **4** appears to be the first example of $[\text{Ru}(\eta^3\text{-allyl})\text{Cl}(\text{CO})(\text{PPh}_3)_2]$ with a terminal substituent anti to the central allyl proton or substituent. Complex **4** exists as two isomers (**4A** and **4B**) in solution, as indicated by the NMR spectroscopic data (see discussion below).

In solution and in the solid state, complex **4** slowly isomerizes to the known allyl complex **5** (Scheme 1), which was prepared previously alternatively from the reaction of $\text{RuHCl}(\text{CO})(\text{PPh}_3)_3$ with isoprene.^{5d} The structure of **5** has been confirmed by X-ray diffraction studies. The molecular structure of **5** is shown in Figure 1. The crystallographic details and selected bond distances and angles are given in Tables 1 and 2, respectively. The structure of complex **5** can be described as a trigonal bipyramid with the two PPh_3 groups and the allyl ligand at the equatorial positions and the Cl and CO ligands at the axial positions. The $\text{P}(1)\text{-Ru}(1)\text{-P}(2)$ angle is $107.73(3)^\circ$. The allyl complex is in the endo

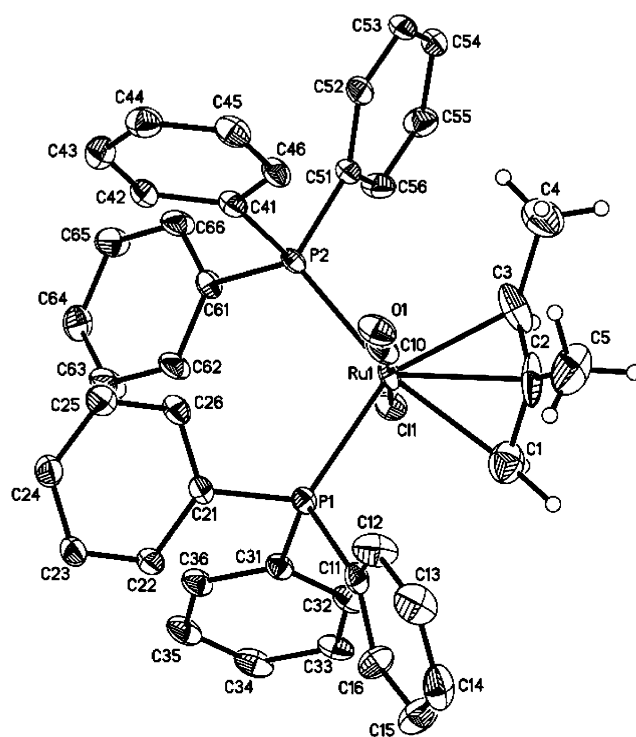


Figure 1. Molecular structure of $[\text{Ru}(\eta^3\text{-CH}_2\text{CMeCHMe})\text{Cl}(\text{CO})(\text{PPh}_3)_2]$.

form, in which the methyl on the central allylic carbon points toward the CO. The C–C bond distances of the allyl ligand together with Ru–C(allyl) are similar to those of reported ruthenium allyl complexes.^{1b–d,g,7}

A proposed mechanism for the isomerization of **4** to **5** is shown in Scheme 2. The bonding mode of the allyl ligand in complex **4** can change from η^3 to η^1 to give intermediate **A**, which could undergo β -H elimination to give intermediate **B** and then **C**. Intermediate **C** could undergo an insertion reaction to give **5**.

NMR Properties of Complex 4. At room temperature, both the ^{31}P and the ^1H NMR spectra of **4** exhibit broad peaks, indicating that the complex is fluxional. To study the fluxional behavior, VT NMR experiments were carried out. As an illustration, the variable-temperature (298 to 242 K) $^{31}\text{P}\{^1\text{H}\}$ NMR spectra (in toluene- d_8) are shown in Figure 2. In the room-temper-

Scheme 2

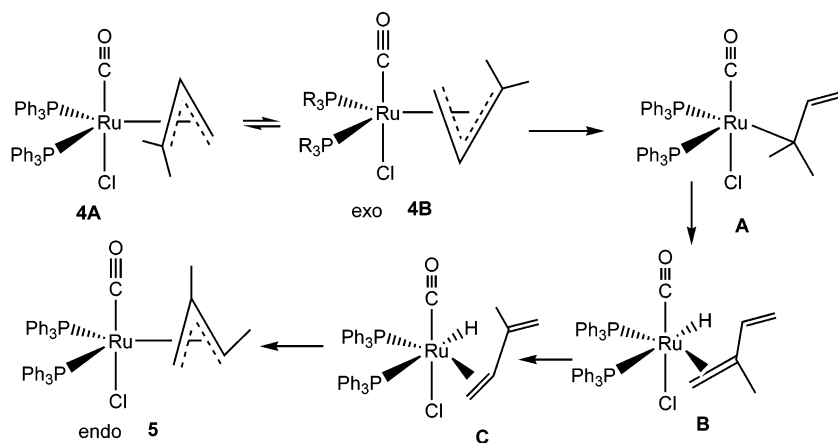


Table 1. Crystal Data and Structure Refinement Details for $[\text{Ru}(\eta^3\text{-CH}_2\text{CMeCHMe})\text{Cl}(\text{CO})(\text{PPh}_3)_2]$ (5)

formula	$\text{C}_{42}\text{H}_{39}\text{ClOP}_2\text{Ru}$
fw	758.19
cryst syts	triclinic
space group	$P\bar{1}$
a , Å	9.9594(10)
b , Å	10.1567(10)
c , Å	18.8676(18)
α , deg	87.811(2)
β , deg	82.016(2)
γ , deg	67.2980(10)
V , Å ³	1743.4(3)
Z	2
d_{calcd} , g cm ⁻³	1.444
θ range, deg	2.17–25.00
no. of rflns collected	11 918
no. of indep rflns	5915 ($R(\text{int}) = 0.0293$)
no. of data/restraints/params	5915/0/424
final R indices ($I > 2\sigma(I)$), %	$R1 = 4.60, wR2 = 11.25$
goodness of fit	1.038
largest diff peak, e Å ⁻³	1.004
largest diff hole, e Å ⁻³	-0.896

Table 2. Selected Bond Lengths (Å) and Angles (deg) for $[\text{Ru}(\eta^3\text{-CH}_2\text{CMeCHMe})\text{Cl}(\text{CO})(\text{PPh}_3)_2]$ (5)

Ru(1)–C(10)	1.813(5)	Ru(1)–C(2)	2.245(4)
Ru(1)–C(3)	2.261(5)	Ru(1)–C(1)	2.276(5)
Ru(1)–P(1)	2.3985(10)	Ru(1)–P(2)	2.3996(10)
Ru(1)–Cl(1)	2.4852(10)	O(1)–C(10)	1.105(5)
C(1)–C(2)	1.399(8)	C(2)–C(3)	1.396(9)
C(2)–C(5)	1.536(7)	C(3)–C(4)	1.506(8)
C(10)–Ru(1)–C(2)	84.94(19)	C(10)–Ru(1)–C(3)	98.57(19)
C(2)–Ru(1)–C(3)	36.1(2)	C(10)–Ru(1)–C(1)	101.25(19)
C(2)–Ru(1)–C(1)	36.1(2)	C(3)–Ru(1)–C(1)	64.8(2)
C(10)–Ru(1)–P(1)	88.58(13)	C(2)–Ru(1)–P(1)	119.1(2)
C(3)–Ru(1)–P(1)	152.10(17)	C(1)–Ru(1)–P(1)	87.41(14)
C(10)–Ru(1)–P(2)	93.71(14)	C(2)–Ru(1)–P(2)	133.07(19)
C(3)–Ru(1)–P(2)	98.73(17)	C(1)–Ru(1)–P(2)	159.04(15)
P(1)–Ru(1)–P(2)	107.73(3)	C(10)–Ru(1)–Cl(1)	176.97(14)
P(1)–Ru(1)–Cl(1)	90.98(3)	P(2)–Ru(1)–Cl(1)	83.57(3)
C(2)–C(1)–Ru(1)	70.8(3)	C(3)–C(2)–C(1)	120.7(5)
C(3)–C(2)–C(5)	121.2(5)	C(1)–C(2)–C(5)	117.9(6)
C(3)–C(2)–Ru(1)	72.6(3)	C(1)–C(2)–Ru(1)	73.2(3)
C(5)–C(2)–Ru(1)	121.9(4)	C(2)–C(3)–C(4)	124.6(5)
C(2)–C(3)–Ru(1)	71.3(3)	C(4)–C(3)–Ru(1)	128.8(4)
O(1)–C(10)–Ru(1)	177.3(4)		

ature (298 K) $^{31}\text{P}\{^1\text{H}\}$ NMR spectrum, complex 4 exhibits a broad peak at 35 ppm (the two minor doublets marked with asterisks at 31.7 (d, $J = 2.7$ Hz) and 38.5 ppm are due to $[\text{Ru}(\eta^3\text{-CH}_2\text{CMeCHMe})\text{Cl}(\text{CO})(\text{PPh}_3)_2]$ (5), which was formed by the isomerization of 4 as described above). When the temperature is increased

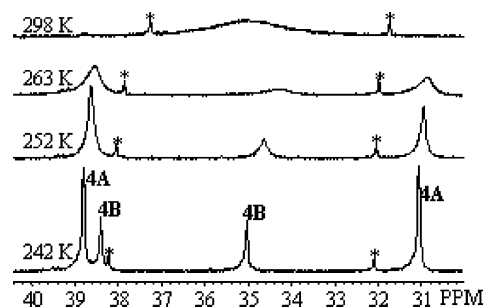
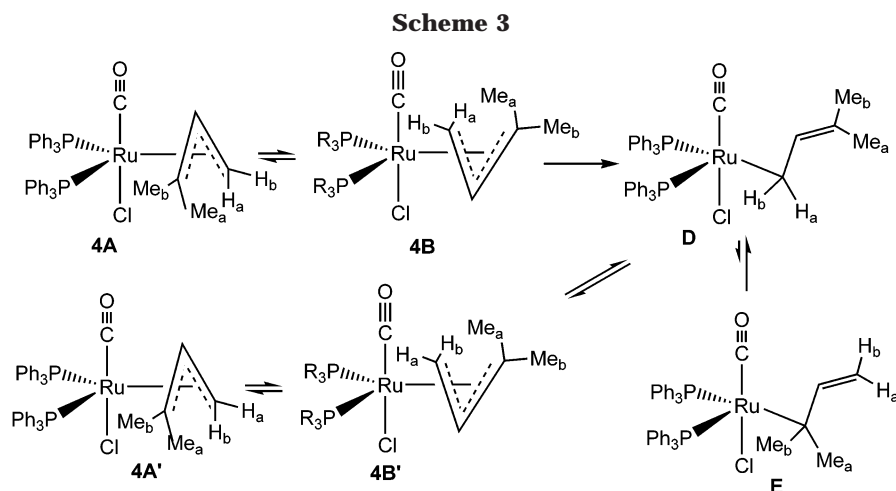


Figure 2. Variable-temperature $^{31}\text{P}\{^1\text{H}\}$ NMR spectra of $[\text{Ru}(\eta^3\text{-CH}_2\text{=CHCMe}_2)\text{Cl}(\text{CO})(\text{PPh}_3)_2]$ in $\text{toluene-}d_8$. The signals marked with an asterisk are due to $[\text{Ru}(\eta^3\text{-CH}_2\text{-CMeCHMe})\text{Cl}(\text{CO})(\text{PPh}_3)_2]$.

to 50 °C, the broad signal changes to a sharp singlet at 34.6 ppm. When the temperature is lowered to 263 K, the broad peak observed at room temperature is separated into three broad peaks at 30.9, 34.2, and 38.6 ppm. On further lowering of the temperature, these peaks become sharp and then change to four signals at 30.1, 35.0, 38.4, and 38.8 ppm when the temperature reaches 242 K. The major signals at 30.1 and 38.8 ppm are associated with each other with a coupling constant of 3.6 Hz, while the minor signals at 35.0 and 38.4 ppm are associated with each other with no resolvable coupling. The NMR data indicate that the allyl complex $[\text{Ru}(\eta^3\text{-CH}_2\text{CHCMe}_2)\text{Cl}(\text{CO})(\text{PPh}_3)_2]$ (4) exists as two isomers which are in fast equilibrium in solution. The more intense ^{31}P signals at 242 K at 30.1 and 38.8 ppm can be attributed to the endo isomer 4A, and the minor signals at 35.0 and 38.4 ppm can be attributed to the exo isomer 4B. Two ^{31}P signals for each of the isomers are expected because of the presence of the unsymmetrical allyl ligand. The observation of a single ^{31}P signal in the $^{31}\text{P}\{^1\text{H}\}$ NMR spectra at room temperature or above can be explained by the fast interconversion of the isomers via η^1 -allyl intermediates.

The fluxional behavior is also reflected in the VT ^1H NMR spectrum. At 213 K, the ^1H NMR spectrum showed the proton signals of the allyl group of 4A at 1.38 (3 H, CH₃), 1.88 (3 H, CH₃), 3.16 (1 H, CH₂), 3.51 (1 H, CH₂), and 4.96 (central CH) ppm and those of 4B at 1.19 (3 H, CH₃), 1.65 (3 H, CH₃), 2.95 (1 H, CH₂), 3.31 (1 H, CH₂), and 5.75 (1 H, central CH) ppm. On the basis of the ^1H NMR integration, the ratio of 4A to 4B was estimated to be 2.4:1. The ^1H NMR spectrum



at room temperature showed only one set of proton signals for the allyl group at 1.30 (3 H, CH₃), 1.66 (3 H, CH₃), 3.08 (2 H, CH₂), and 5.21 (1 H, central CH) ppm. The NMR data suggest that the two terminal CH₂ protons are exchanging more rapidly than the two terminal CMe₂ methyl groups, and the fluxional behavior can be explained by the mechanism shown in Scheme 3. A similar mechanism was proposed previously for the interconversion of endo and exo isomers of [(MeSi(CH₂-PMe₂)₃)RuMe(η³-CH₂CMeCH₂)].⁸

NMR Properties of Complexes 5 and 6. In contrast to **4**, only the endo isomer can be detected by ¹H and ³¹P NMR in solution for the complex [Ru(η³-CH₂-CMeCHMe)Cl(CO)(PPh₃)₂] (**5**). In addition, the ¹H and ³¹P NMR signals are sharp at room temperature, indicating that the complex is not fluxional at this temperature. We have also carefully examined the ³¹P and ¹H NMR spectra of the related complex [Ru(η³-CH₂-CHCHPh)Cl(CO)(PPh₃)₂] (**6**),^{5a} which was prepared from the reaction of **3** with CH₂=C=CHPh. Like [Ru(η³-CH₂-CMeCHMe)Cl(CO)(PPh₃)₂] (**5**), the ³¹P{¹H} NMR spectrum of [Ru(η³-CH₂-CHCHPh)Cl(CO)(PPh₃)₂] (**6**) at room temperature (298.7 K) showed two sharp doublets at 26.5 and 38.9 ppm with a coupling constant of 5.1 Hz, indicating that the complex is not fluxional and has only one isomer observable by NMR at this temperature. Consistent with this proposition, the room-temperature ¹H NMR spectrum showed four allylic proton signals at 3.26 (CH₂), 3.61 (CH₂), 4.61 (CHPh), and 5.85 (central CH) ppm. We also carried out VT ¹H and ³¹P{¹H} NMR experiments for the compound, and the exo isomer was also not observed in the temperature range 298–363 K in toluene.

Theoretical Study. It is interesting to note that two isomers are observed for [Ru(η³-CH₂CHCMe₂)Cl(CO)(PPh₃)₂], but only one isomer is observed for other related allyl complexes [Ru(η³-CH₂CMeCHMe)Cl(CO)(PPh₃)₂] and [Ru(η³-CH₂CHCHPh)Cl(CO)(PPh₃)₂]. To better understand the substituent effect on the behavior, a computational study has been carried out.

Before exploring the substituent effect on the isomerism of substituted-allyl complexes, we first discuss the isomeric behavior of the η³-allyl complex [Ru(η³-CH₂-CHCH₂)Cl(CO)(PPh₃)₂], a model complex for [Ru(η³-CH₂-

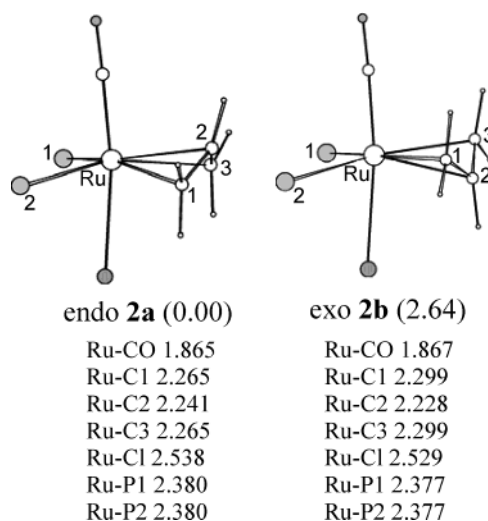


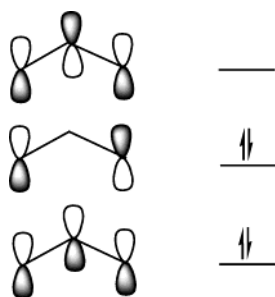
Figure 3. B3LYP optimized structures of **2a** and **2b** together with selected bond distances (in Å) and relative energies (in parentheses, in kcal/mol). For clarity, the hydrogen atoms of PH₃ are omitted.

CHCH₂)Cl(CO)(PPh₃)₂]. Figure 3 shows the endo and exo structures calculated for the model η³-allyl complex [Ru(η³-CH₂-CHCH₂)Cl(CO)(PPh₃)₂] together with selected bond distances. The endo isomer (**2a**) is lower in energy than the exo one (**2b**) by 2.64 kcal/mol, from which the ratio of the endo and exo isomers is calculated to be 86:1 at room temperature (298.15 K) according to the Boltzmann distribution. Such a large ratio implies that the amount of the exo isomer is too small to be detected easily by NMR in solution, consistent with the experimental observations mentioned above.^{5–7} Here, we purposely label the structures with lower-case letters to distinguish them from those described in the Experimental Section, which are labeled with upper-case letters.

Clearly, the relative stabilities of the endo and exo isomers determine whether both isomers of the η³-allyl complex can be detected in solution. The question now is what factors determine the relative stability of the two isomers. Comparing the two calculated structures (Figure 3), we can see that the two structures have similar Ru–CO, Ru–P, and Ru–Cl bond distances. However, noticeable differences between the two structures can be found in the bond distances associated with

(8) McNeill, K.; Anderson, R. A.; Bergman, R. G. *J. Am. Chem. Soc.* **1997**, *119*, 11244.

Scheme 4

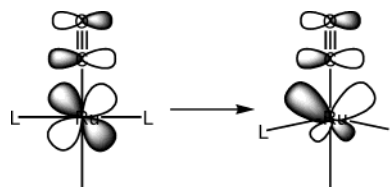

Table 3. Results of Natural Bond Order and Population Analyses for $[Ru(\eta^3\text{-CH}_2\text{CHCH}_2)Cl(CO)(PPh_3)_2]$

isomer	Wiberg bond index		natural atomic charge	
	Ru–C(terminal)	Ru–C(central)	C(terminal)	C(central)
2a (endo)	0.4004	0.1718	–0.361	–0.105
2b (exo)	0.3764	0.1831	–0.350	–0.109

the Ru– η^3 -allyl structural units. The Ru–C(terminal) bonds (between Ru and the terminal carbons of the η^3 -allyl ligand) in the endo isomer are stronger than those in the exo isomer. In contrast, the Ru–C(central) bond in the exo isomer is stronger than that in the endo isomer. The greater stability of the endo isomer is apparently related to its stronger Ru–C(terminal) bonds. In contrast, the stronger Ru–C(central) bond in the exo isomer does not render its stability. The reason for this unusual behavior can be explained as follows. An η^3 -allyl ligand is generally considered as a monoanionic ligand. One of the two orbitals accommodating the four π electrons of the η^3 -allyl anionic ligand has no orbital contribution from the central carbon (Scheme 4).⁹ Therefore, the central carbon of the η^3 -allyl ligand makes a smaller contribution to the Ru– η^3 -allyl bonding interactions in comparison to the two terminal carbons, although the Ru–C(central) bond is always shorter than the Ru–C(terminal) bonds for a given η^3 -allyl complex. Natural bond order (NBO) analyses indeed give a much smaller Wiberg bond index for the Ru–C(central) bond in comparison to the Ru–C(terminal) bonds (Table 3).

The calculated structural features of isomers of the model complex $[Ru(\eta^3\text{-CH}_2\text{CHCH}_2)Cl(CO)(PPh_3)_2]$ indicate that the endo isomer has stronger Ru–C(terminal) bonds than the exo isomer. Thus, stronger Ru– η^3 -allyl bonding interactions are expected for the endo isomer, because the Ru–C(central) bond makes a relatively small contribution to the structural stability. A plausible explanation for the weaker Ru–C(terminal) bonds in the exo isomer is given below. In a carbonyl complex, the ligands that are cis to CO are normally expected to bend away from the carbonyl ligand in order to maximize the M(d)-to-CO(π^*) back-bonding interaction. In other words, large angles between CO and its cis ligands would increase the back-bonding interaction. Scheme 5 illustrates the d–p orbital mixing, showing the increased orbital overlap due to the bending of angles. The mixing of metal p orbitals with d orbitals is commonly employed to explain the enhancement of metal(d)-to-ligand(π^*) back-bonding interactions.¹⁰ In the endo isomer, the two

Scheme 5



Ru–C(terminal) bonds form larger angles (100.7°) with CO. The optimal structural arrangement for bonding interactions is achieved, and therefore, the Ru–C(terminal) bonds are relatively stronger. In the exo isomer, the two Ru–C(terminal) bonds have quite small angles (88.3°) with the CO ligand. This structural arrangement does not provide an optimal situation to maximizing the Ru(d)-to-CO(π^*) back-bonding interaction. Thus, the optimal structural arrangement is not met. The overall effect in maintaining the Ru–CO interaction is the weakening of the Ru–C(terminal) bonds. We can conclude that the greater stability of the endo isomer is related to its stronger Ru–C(terminal) bonds due to relatively less weakening caused by the cis Ru–CO bond.

To understand how substituents on the η^3 -allyl ligand affect the relative stabilities of the endo and exo isomers, we discuss the isomerism of monomethyl-substituted η^3 -allyl complexes. Figure 4 shows six isomeric structures calculated for the monomethyl-substituted η^3 -allyl complex. In the endo (**7a**) and exo (**7b**) isomers, the methyl substituent is syn with respect to the substituent at the central carbon of the allyl ligand, while in the endo (**7a'**) and exo (**7b'**) isomers, the methyl substituent is anti with respect to the substituent at the central carbon of the allyl ligand. In the endo (**7a''**) and exo (**7b''**) isomers, the methyl substituent is at the central C2 atom of the allyl ligand. The energy difference between **7a** and **7b** (2.52 kcal/mol) is close to that between **2a** and **2b** (2.64 kcal/mol), indicating that the syn-methyl substituent has a negligible effect on the energy difference between the endo and exo isomers. The C4–C1–Ru–C5 dihedral angle in **7a** is 47.4° and the C4–C1–Ru–Cl angle in **7b** is 48.5° , giving staggered arrangements of the methyl substituent with respect to the Ru–CO or Ru–Cl and Ru– PPh_3 bonds. The staggered arrangements in **7a** and **7b** minimize the steric repulsion caused by the methyl substituent and are clearly responsible for the negligible effect. For **7a'** and **7b'**, which have an anti methyl substituent, the energy difference (0.77 kcal/mol) between the endo (**7a'**) and exo (**7b'**) isomers is much smaller than that between **2a** and **2b** (2.64 kcal/mol), indicating that the anti methyl substituent has a significant effect on the energy difference. The C4–C1–Ru–Cl dihedral angle in **7a'** is 5.3° and the C4–C1–Ru–C5 one in **7b'** is 2.1° , giving eclipsed arrangements of the methyl substituent with respect to the Ru–Cl or Ru–CO bond. Clearly, steric repulsion due to the eclipsed arrangements is expected to destabilize both the endo (**7a'**) and exo (**7b'**) isomers. The relatively small energy difference between **7a'** and **7b'** in comparison to that between **2a** and **2b**, which do not have a methyl substituent, suggests that the destabilization in **7b'** is more significant than in **7a'**. In other words, the 1,4-repulsion between a methyl group and a chloride ligand is greater than that between a methyl group and a

(9) Crabtree, R. H. *The Organometallic Chemistry of the Transition Metals*, 3rd ed.; Wiley: New York, 2001; p 122.

(10) Albright, T. A.; Burdett, J. K.; Whangbo, M.-H. *Orbital Interactions in Chemistry*; Wiley: New York, 1985; p 321.

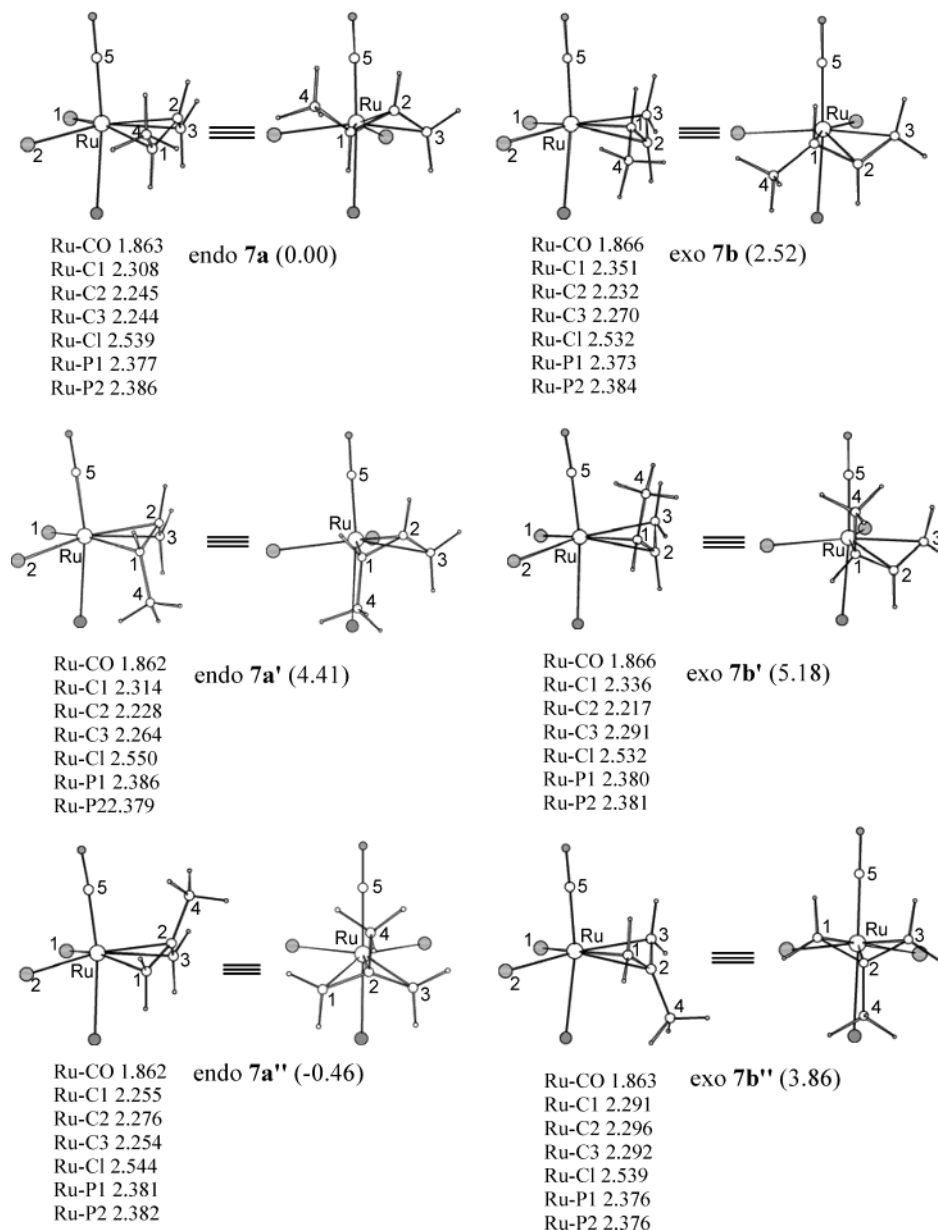


Figure 4. B3LYP optimized structures of the monomethyl-substituted η^3 -allyl complex together with selected bond distances (in Å) and relative energies (in parentheses, in kcal/mol). For clarity, the hydrogen atoms of PH_3 are omitted.

carbonyl ligand. A plausible explanation for this observation is that the negative charge carried by the chloride exerts a greater repulsive force. Further support to the plausible explanation comes from the energy difference calculated for **7a''** and **7b''**. The methyl substituent eclipses the Ru-CO bond in **7a''** and the Ru-Cl bond in **7b''**. The increased energy difference between **7a''** and **7b''** is clearly a result of the large steric repulsion between the methyl substituent and the Ru-Cl bond in **7b''**.

Supports to the steric argument above can also be found from our additional calculations on the relative stabilities of the endo and exo isomers having an anti substituent bulkier than methyl, such as *tert*-butyl. **7a'** (endo) is more stable than **7b'** (exo) by 0.77 kcal/mol. When the methyl groups in **7a'** and **7b'** are replaced by *tert*-butyl, the stability order is reversed, the exo isomer being more stable than the endo isomer by 1.29 kcal/mol. **7a** is more stable than **7a'** by 4.41 kcal/mol, while **7b** is more stable than **7b'** by 2.66 kcal/mol. For the

methyl-substituted free allyl, the syn form adopted by **7a** and **7b** was calculated to be more stable by only ca. 1.0 kcal/mol than the anti form adopted by **7a'** and **7b'**. These results suggest that the eclipsed arrangements in **7a'** and **7b'** (with respect to Ru-Cl and Ru-CO, respectively) contribute significantly to their instability.

Figure 5 shows four isomeric structures calculated for the dimethyl-substituted η^3 -allyl model complex. In the endo (**4a**) and exo (**4b**) isomers, the two methyl substituents are at the same terminal carbon atom of the η^3 -allyl ligand, while in the endo (**5a**) and exo (**5b**) isomers one methyl substituent is at one terminal carbon and the other is at the central one. The results of calculations show that the exo (**4b**) isomer is higher in energy than the endo (**4a**) one only by 0.25 kcal/mol (**4a:4b** = 100:66, 298.15 K), consistent with the experimental observations that both the endo and exo isomers coexist in solution. From the discussion above, we know that a syn-methyl substituent has a negligible effect on the energy difference between the endo and exo isomers.

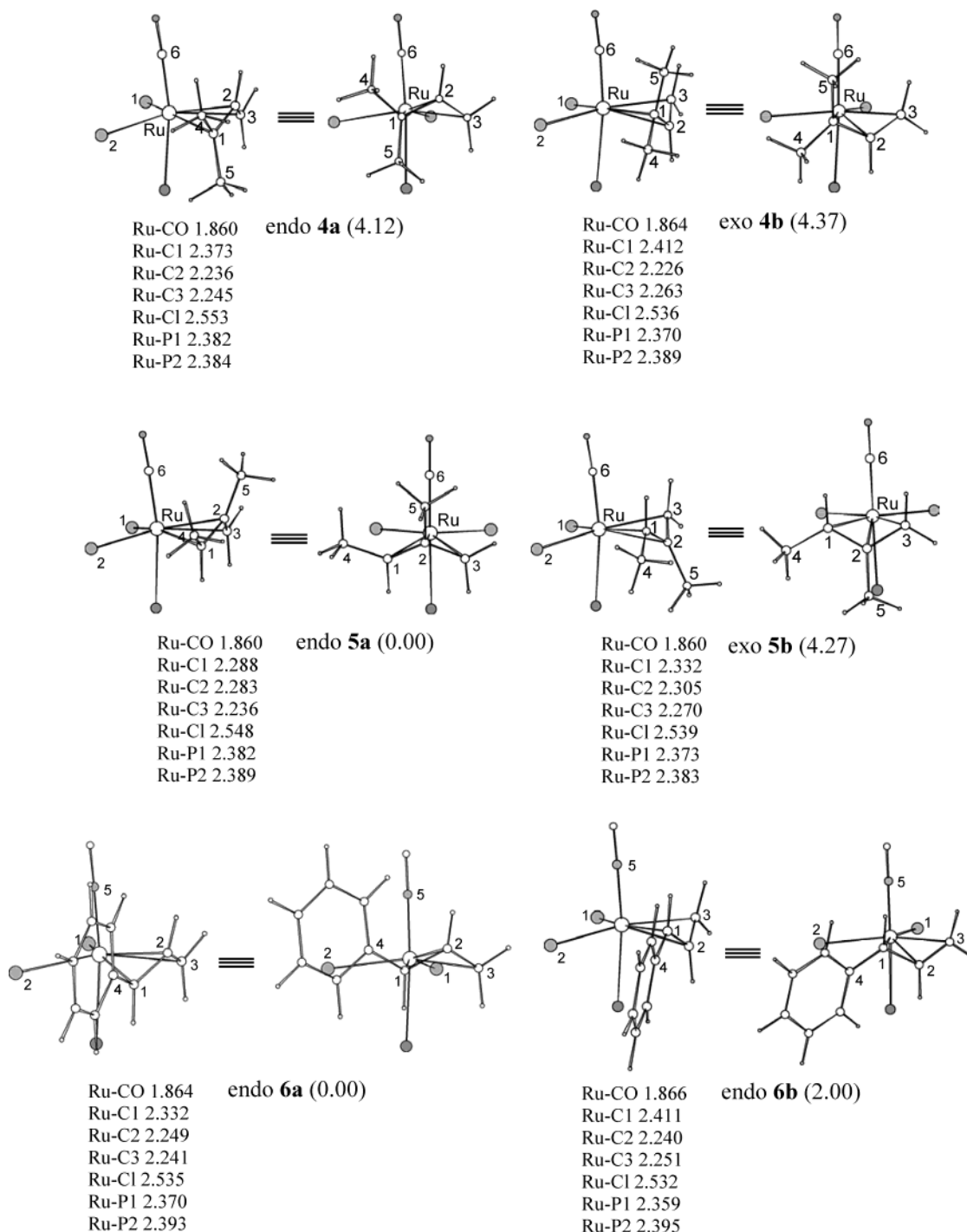


Figure 5. B3LYP optimized structures of the dimethyl-substituted η^3 -allyl complex together with selected bond distances (in Å) and relative energies (in parentheses, in kcal/mol). For clarity, the hydrogen atoms of PH_3 are omitted.

Therefore, the energy difference between **4a** and **4b** is small, similar to that found between **7a'** and **7b'**, because an anti substituent destabilizes the endo isomer (**4a** or **7a'**) more in comparison to the exo isomer (**4b** or **7b'**). Experiments described above show that isomers **4A** and **4B** slowly isomerize to **5** having an endo structural form. Our calculations indeed show that **5a** is the most stable among the four isomers (Figure 5). For **5a** and **5b**, the energy difference (4.27 kcal/mol) is large. These results are again consistent with the experimental observation that only one isomer was observed by NMR in solution. The energy difference between **5a** and **5b** is also similar to that found between

7a'' and **7b''**, consistent with the notion that a syn substituent has a negligible effect on the energy difference, due to its staggered arrangements with respect to the Ru-CO or Ru-Cl and Ru- PH_3 bonds.

Calculations were also done for $[\text{Ru}(\eta^3\text{-CH}_2\text{CHCHPh})\text{Cl}(\text{CO})(\text{PH}_3)_2]$, a model complex of **6**. The energy difference between the endo (**6a**) and exo (**6b**) isomers was found to be 2.00 kcal/mol (Figure 5), comparable to that between **2a** and **2b**, although it is slightly smaller. The argument used to understand the energy difference between **2a** and **2b** can be applied here also. Experiments detect only the endo isomer of **6**, suggesting that

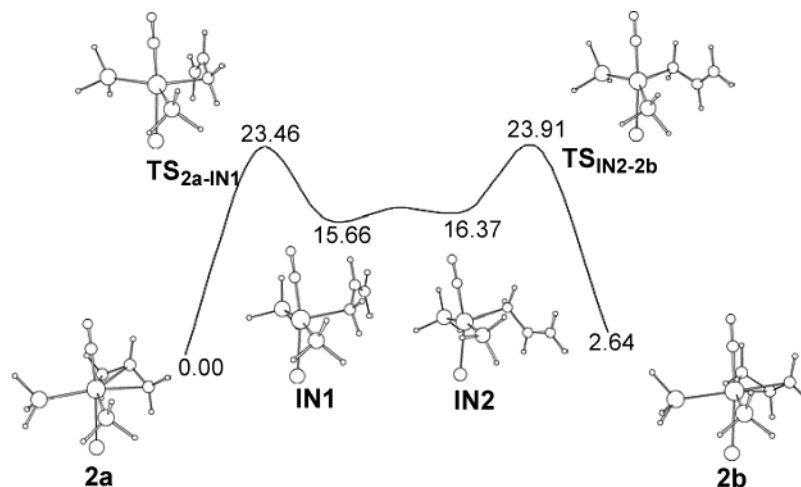


Figure 6. Energy profile for the **2a(exo)** → **2b(endo)** interconversion process.

the amount of the exo isomer is too small to be detected under the experimental conditions.

The mechanism of the exo–endo interconversion is another interesting point to be addressed computationally. The calculations support our proposal that η^1 -allyl intermediates are involved in the interconversion process. Figure 6 shows the energy profile for the **2a(exo)** → **2b(endo)** process. Rearrangement of η^3 -allyl in **2a** to η^1 -allyl in the intermediate **IN1** requires a barrier of 23.46 kcal/mol. A barrierless rotation of the η^1 -allyl ligand along the Ru– η^1 -allyl bond in **IN1** gives another η^1 -allyl intermediate, **IN2**. **IN2** differs from **IN1** only in the orientation of the η^1 -allyl ligand. Formation of the endo isomer **2b** from **IN2** requires a barrier of only 7.54 kcal/mol. An attempt to locate transition states for the possible mechanism involving a direct η^3 -allyl rotation failed. Keeping the η^3 -allyl bonding mode with constrained geometry optimizations, we obtained a series of η^3 -allyl structures along the direct rotation path. From these partially optimized structures, transition states were searched. These calculations gave either the local minima we have already obtained or the transition states that are relevant to the mechanism presented in Figure 6. Therefore, a direct η^3 -allyl rotation for the exo–endo interconversion seems unlikely.

Conclusions

The allyl complex $[\text{Ru}(\eta^3\text{-CH}_2\text{CHCMe}_2)\text{Cl}(\text{CO})(\text{PPh}_3)_2]$ has been prepared from the reaction of $\text{CH}_2=\text{C}=\text{CMe}_2$ with $[\text{RuHCl}(\text{CO})(\text{PPh}_3)_3]$. In solution, both endo and exo isomers were observed by NMR for the new allyl complex $[\text{Ru}(\eta^3\text{-CH}_2\text{CHCMe}_2)\text{Cl}(\text{CO})(\text{PPh}_3)_2]$. In contrast, only one isomer was detected for other related analogous allyl complexes $[\text{Ru}(\eta^3\text{-allyl})\text{Cl}(\text{CO})(\text{PPh}_3)_2]$ (e.g. allyl = $\text{CH}_2\text{CMeCHMe}$, CH_2CHCHPh). The theoretical calculations show that, for the $[\text{Ru}(\eta^3\text{-allyl})\text{Cl}(\text{CO})(\text{PR}_3)_2]$ complexes, the metal– η^3 -allyl interaction in an endo isomer is stronger than that in an exo isomer. In the endo isomer, the two Ru–C(terminal) bonds form larger angles with the CO ligand and are stronger because the structural arrangement provides an optimal situation to maximize the Ru(d)-to-CO(π^*) back-bonding interaction. Intrinsically, an endo isomer is expected to be more stable than its exo form. However, substituents

at the η^3 -allyl ligand also play an important role in determining the relative stability. We found that an anti substituent at one of the terminal carbons destabilizes the endo isomer more significantly and therefore makes the endo and exo isomers comparable in terms of their relative stability. The comparable stability allows both isomers to be observable in solution. A syn substituent is, however, found to have a negligible effect on the relative stability. The endo–exo interconversion was found to proceed by intervention of η^1 -allyl intermediates instead of a direct η^3 -allyl rotation.

Experimental Section

All manipulations were carried out under a nitrogen atmosphere using standard Schlenk techniques, unless otherwise stated. Solvents were distilled under nitrogen from sodium benzophenone (hexane, ether, THF), sodium (benzene), or calcium hydride (CH_2Cl_2). The starting materials $[\text{RuHCl}(\text{CO})(\text{PPh}_3)_3]$ ¹¹ and phenylallene¹² were prepared according to the literature methods. All other reagents were used as purchased from Aldrich Chemical Co.

Microanalyses were performed by M-H-W Laboratories (Phoenix, AZ). ¹H, ¹³C{¹H}, and ³¹P{¹H} NMR spectra were collected on a Bruker ARX-300 spectrometer (300 MHz). ¹H and ¹³C NMR shifts are relative to TMS, and ³¹P chemical shifts are relative to 85% H_3PO_4 .

[Ru(η^3 -CH₂CHCMe₂)Cl(CO)(PPh₃)₂] (4). To a stirred solution of $[\text{RuHCl}(\text{CO})(\text{PPh}_3)_3]$ (0.512 g, 0.538 mmol) in dichloromethane (24 mL) was added dropwise a solution of 3-methyl-1,2-butadiene (0.054 mL, 0.54 mmol) in dichloromethane (9 mL) at room temperature. After the addition was complete, the resulting mixture was stirred for 20 min. The volatile materials were then removed under vacuum. Addition of diethyl ether (5 mL) to the residue gave an orange solid, which was collected by filtration, washed with ether (5 mL × 3), a mixture of THF/ether (1:4 v/v, 5 mL), and hexane (5 mL × 2) in turn, and then dried under vacuum. Yield: 342 mg, 84%. ¹H NMR (300 MHz, CD_2Cl_2 , 298 K): δ 0.81 (s, 3 H, CH_3), 1.29 (s, 3 H, CH_3), 2.52 (br d, $J(\text{HH}) = 10.1$ Hz, 2 H, CH_2), 4.77 (br t, $J(\text{HH}) = 10.1$ Hz, 1 H, central CH), 7.15–7.30 (m, 18 H, phenyl), 7.35–7.41 (m, 12 H, phenyl). ³¹P{¹H} NMR (121.5 MHz, CD_2Cl_2 , 298 K): δ 35.8 (br). ¹H NMR (300 MHz, toluene-*d*₈, 299 K): δ 1.30 (br s, 3 H, CH_3), 1.66 (br s, 3 H, CH_3), 3.08 (d, $J(\text{HH}) = 9.9$ Hz, 2 H, CH_2), 5.21 (br t, $J(\text{HH}) =$

(11) Ahmad, N.; Levison, J. J.; Robinson, S. D.; Uttley, M. F.; Wonchoba, E. R.; Parshall, G. W. *Inorg. Synth.* **1974**, *15*, 45.

(12) Trost, B. M.; Pinkerton, A. B.; Seidel, M. *J. Am. Chem. Soc.* **2001**, *123*, 12466.

9.9 Hz, 1 H, central CH), 7.20 (m, 18 H, phenyl), 7.88 (m, 12 H, phenyl). $^{31}\text{P}\{^1\text{H}\}$ NMR (121.5 MHz, toluene- d_6 , 298 K): δ 35.0 (br). Selected ^1H NMR data of **4A** at 213 K (300 MHz, toluene- d_6): δ 1.38 (br s, 3 H, CH_3), 1.88 (br s, 3 H, CH_3), 3.16 (br s, 1 H, CH_2); 3.51 (br d, $J(\text{HH}) = 11.8$ Hz, 1 H, CH_2), 4.96 (br m, 1 H, central CH). Selected ^1H NMR data of **4B** at 213 K (300 MHz, toluene- d_6): δ 1.19 (br s, 3 H, CH_3), 1.65 (br s, 3 H, CH_3), 2.95 (br d, $J(\text{HH}) = 10.8$ Hz, 1 H, CH_2), 3.31 (br s, 1 H, CH_2), 5.75 (br m, 1 H, central CH). $^{31}\text{P}\{^1\text{H}\}$ NMR (121.5 MHz, toluene- d_6 , 213 K): δ 31.3 (d, $J(\text{PP}) = 3.8$ Hz, **4A**), 36.1 (s, **4B**), 38.0 (s, **4B**), 39.3 (d, $J(\text{PP}) = 3.8$ Hz, **4A**). Anal. Found: C, 66.91; H, 5.29. Calcd for $\text{C}_{42}\text{H}_{39}\text{ClO}_2\text{Ru}$: C, 66.53; H, 5.18.

$[\text{Ru}(\eta^3\text{-CH}_2\text{CMeCHMe})\text{Cl}(\text{CO})(\text{PPh}_3)_2]$ (5**).** A solution of $[\text{Ru}(\eta^3\text{-CH}_2\text{CHCMe}_2)\text{Cl}(\text{CO})(\text{PPh}_3)_2]$ (35.4 mg) in toluene (4 mL) was heated at 60 °C for 4 h. After the solvent was removed under vacuum, the residue was washed with diethyl ether and hexane in turn and dried in vacuo. Yield: 10.5 mg, 30%. Compound **5** was also obtained in 41% isolated yield when a solution of $[\text{Ru}(\eta^3\text{-CH}_2=\text{CHCMe}_2)\text{Cl}(\text{CO})(\text{PPh}_3)_2]$ (111 mg) in dichloromethane (2 mL) was allowed to stand at ambient temperature for 1 week. ^1H NMR (300 MHz, CD_2Cl_2 , 298 K): δ 0.93 (br s, 3 H, CH_3), 1.89 (s, 3 H, CH_3), 2.60 (d, $J(\text{PH}) = 4.3$ Hz, 1 H, CH_2), 2.67 (br s, 1 H, CH_2), 3.11 (br m, 1 H, CH), 7.18–7.36 (m, 24 H, phenyl), 7.48 (t, 6 H, phenyl). $^{31}\text{P}\{^1\text{H}\}$ NMR (121.5 MHz, CD_2Cl_2 , 298 K): δ 31.7 (d, $J(\text{PP}) = 2.7$ Hz), 38.5 (d, $J(\text{PP}) = 2.7$ Hz).

$[\text{Ru}(\eta^3\text{-CH}_2\text{CHCHPh})\text{Cl}(\text{CO})(\text{PPh}_3)_2]$ (6**).** This complex was prepared from $[\text{RuHCl}(\text{CO})(\text{PPh}_3)_3]$ and phenylallene as a yellow powder, following the procedure for $[\text{Ru}(\eta^3\text{-CH}_2\text{-CHCMe}_2)\text{Cl}(\text{CO})(\text{PPh}_3)_2]$. Yield: 87%. ^1H NMR (300 MHz, toluene- d_6 , 298 K): δ 3.25 (m, 1 H, CH_2), 3.61 (dd, $J(\text{HH}) = 12.4$, $J(\text{PH}) = 5.6$ Hz, CH_2), 4.61 (dd, $J(\text{HH}) = 11.9$, $J(\text{PH}) = 6.7$ Hz, CHPh), 5.85 (m, 1 H, $\text{C}=\text{CHC}$), 7.08–7.22 (m, 23 H, phenyl), 7.76–7.84 (m, 12 H, phenyl). $^{31}\text{P}\{^1\text{H}\}$ NMR (121.5 MHz, toluene- d_6 , 298 K): δ 26.5 (d, $J(\text{PP}) = 5.1$ Hz), 38.9 (d, $J(\text{PP}) = 5.1$ Hz).

Crystal Structure Analyses. Crystals suitable for X-ray diffraction were grown from CH_2Cl_2 solutions of **5** layered with hexane. Data collections were performed on a Bruker Apex CCD area detector, by using graphite-monochromated Mo $K\alpha$ radiation ($\lambda = 0.71073$ Å). Empirical absorption corrections (SADABS) were applied. All structures were solved by direct methods, expanded by difference Fourier syntheses, and refined by full-matrix least squares on F^2 using the Bruker SHELXTL (version 5.10) program package. All non-hydrogen atoms were refined anisotropically. Further details on crystal data, data collection, and refinement are summarized in Table 1.

Computational Details. Molecular geometries of the model complexes were optimized at the Becke3LYP (B3LYP)

level of density functional theory.¹³ Frequency calculations at the same level of theory have also been performed to identify all stationary points as minima (zero imaginary frequency). The LANL2DZ effective core potentials and basis sets¹⁴ were used to describe Ru, Cl, and P, while the standard 6-31G basis set¹⁵ was used for C, H, and O atoms. Polarization functions¹⁶ were also added for C ($\zeta_d = 0.600$), O ($\zeta_d = 1.154$), P ($\zeta_d = 0.340$), and Cl ($\zeta_d = 0.514$). For computational simplicity, the PPh_3 ligand used in experiments was modeled by PH_3 . All calculations were performed with the Gaussian 98 software package.¹⁷

Acknowledgment. We acknowledge financial support from the Hong Kong Research Grants Council (HKUST 6090/02P, HKUST 6087/02P, and DAG03/04.SC15), the University Grants Committee of Hong Kong, through the Area of Excellence Scheme (Aoe).

Supporting Information Available: Tables of bond distances and angles, atomic coordinates and equivalent isotropic displacement coefficients, and anisotropic displacement coefficients for $[\text{Ru}(\eta^3\text{-CH}_2\text{CMeCHMe})\text{Cl}(\text{CO})(\text{PPh}_3)_2]$ (**5**) and Cartesian coordinates of all the calculated structures reported in this article; X-ray data for **5** are also given as a CIF file. This material is available free of charge via the Internet at <http://pubs.acs.org>.

OM049646G

(13) (a) Becke, A. D. *J. Chem. Phys.* **1993**, *98*, 5648. (b) Miehlich, B.; Savin, A.; Stoll, H.; Preuss, H. *Chem. Phys. Lett.* **1989**, *157*, 200. (c) Lee, C.; Yang, W.; Parr, G. *Phys. Rev. B* **1988**, *37*, 785.

(14) (a) Hay, P. J.; Wadt, W. R. *J. Chem. Phys.* **1985**, *82*, 270. (b) Wadt, W. R.; Hay, P. J. *J. Chem. Phys.* **1985**, *82*, 284. (c) Hay, P. J.; Wadt, W. R. *J. Chem. Phys.* **1985**, *82*, 299.

(15) (a) Gordon, M. S. *Chem. Phys. Lett.* **1980**, *76*, 163. (b) Hariharan, P. C.; Pople, J. A. *Theor. Chim. Acta* **1973**, *28*, 213. (c) Binning, R. C., Jr.; Curtiss, L. A. *J. Comput. Chem.* **1990**, *11*, 1206.

(16) Huzinaga, S. *Gaussian Basis Sets for Molecular Calculations*; Elsevier Science: Amsterdam, 1984.

(17) Frisch, M. J.; Trucks, G. W.; Schlegel, H. B.; Scuseria, G. E.; Robb, M. A.; Cheeseman, J. R.; Zakrzewski, V. G.; Montgomery, J. A., Jr.; Stratmann, R. E.; Burant, J. C.; Dapprich, S.; Millam, J. M.; Daniels, A. D.; Kudin, K. N.; Strain, M. C.; Farkas, O.; Tomasi, J.; Barone, V.; Cossi, M.; Cammi, R.; Mennucci, B.; Pomelli, C.; Adamo, C.; Clifford, S.; Ochterski, J.; Petersson, G. A.; Ayala, P. Y.; Cui, Q.; Morokuma, K.; Malick, D. K.; Rabuck, A. D.; Raghavachari, K.; Foresman, J. B.; Cioslowski, J.; Ortiz, J. V.; Stefanov, B. B.; Liu, G.; Liashenko, A.; Piskorz, P.; Komaromi, I.; Gomperts, R.; Martin, R. L.; Fox, D. J.; Keith, T.; Al-Laham, M. A.; Peng, C. Y.; Nanayakkara, A.; Gonzalez, C.; Challacombe, M.; Gill, P. M. W.; Johnson, B. G.; Chen, W.; Wong, M. W.; Andres, J. L.; Head-Gordon, M.; Replogle, E. S.; Pople, J. A. *Gaussian 98*, revision A.9; Gaussian, Inc.: Pittsburgh, PA, 1998.